catalysts

Supplementary

Mn-Ni-Co spinel oxides towards Oxygen Reduction Reaction in Alkaline Medium: $Mn_{0.5}Ni_{0.5}Co_2O_4$/C synergism and cooperation

Thabo Matthews[1], Tarekegn H. Dolla[1], Sandile S. Gwebu[1], Tebogo A. Mashola[1], Lihle T. Dlamini[1], Emanuela Carleschi[2], Patrick Ndungu[1] and Nobanathi W. Maxakato[1,*]

[1]Department of Chemical Sciences, University of Johannesburg, Doornfontein, 2028, South Africa
[2]Department of Chemistry, Wolaita Sodo University, Wolaita Sodo, P. O. Box 138, Ethiopia
[3]Department of physics University of Johannesburg, Auckland Park PO Box 524 Auckland Park 2006, South Africa
* Correspondence: nmaxakato@uj.ac.za; Tel.: +27115596151

S1 Experimental

Experimental

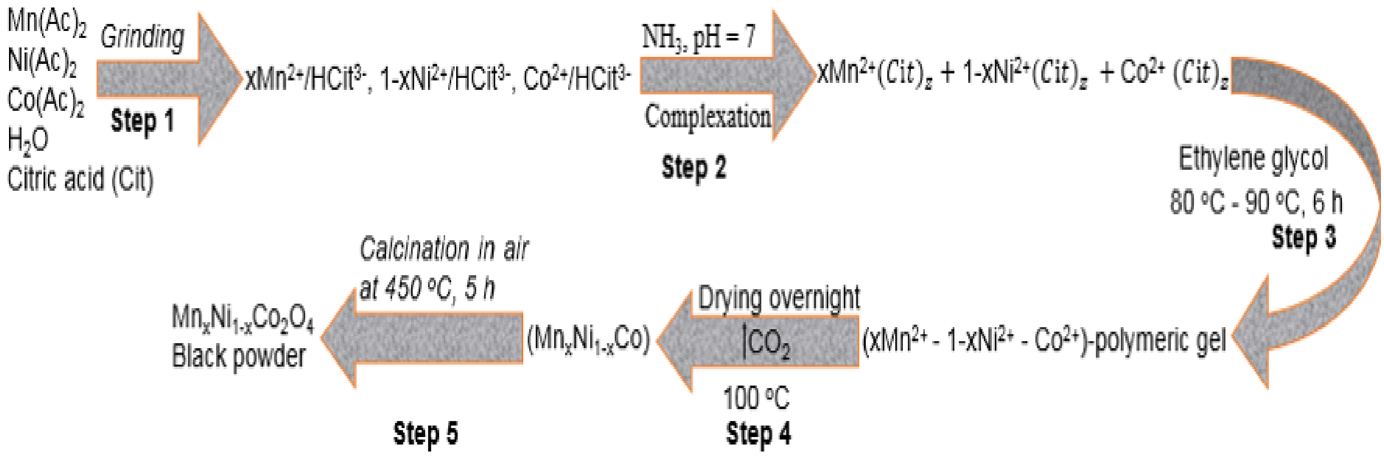

Scheme S1. Formation of $Mn_xNi_{1-x}Co_2O_4$ spinel oxide series

In Step 3, polymeric gel is formed via citrate-ethylene glycol polymerization according to the below:

$$\mathbf{HO(CO)CH_2C(OH)(CO_2H)CH_2CO_2H + HO(CH_2)_2OH \rightarrow HOCH_2CH_2(O)(CO)CH_2C(OH)(CO_2H)CH_2CO_2H + H_2O} \quad \text{Eq. S 1}$$

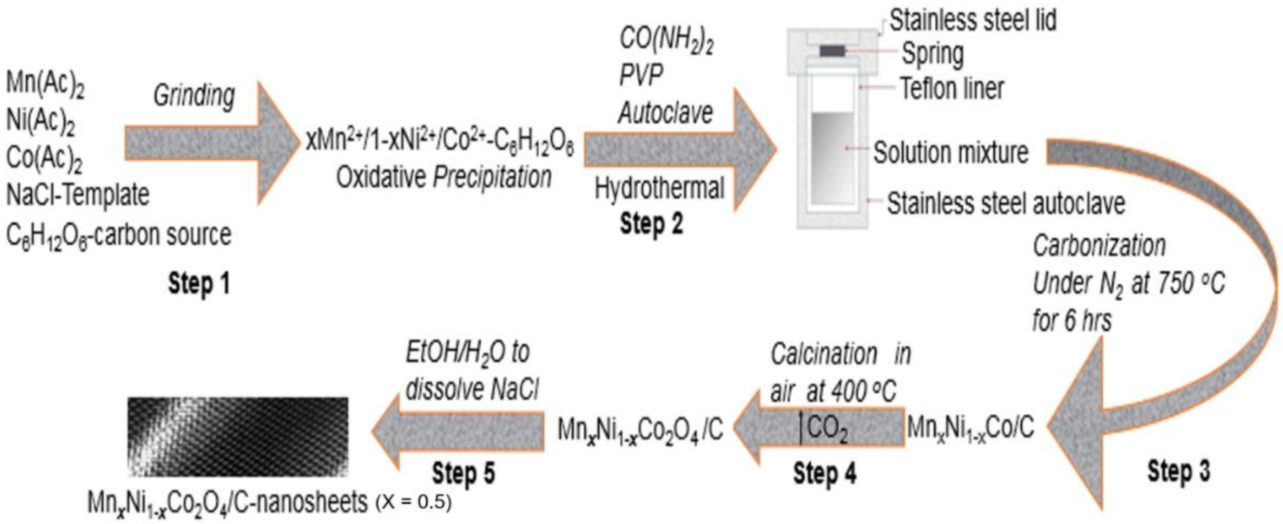

Scheme S2. Formation of $Mn_{0.5}Ni_{0.5}Co_2O_4/C$ using NaCl template.

Tiny residuals of Cl are detected on all samples, as a result of the sample synthesis process and it is worth mentioning that a tiny amount of W was detected on the x=0.7 sample, Fig 4a.

Table S1

BEs (in eV), FWHM (in eV) and relative percentage areas (in %) of the two main components of the Ni 2p core level for the MnNiCoO series and $Mn_{0.5}Ni_{0.5}Co_2O_4/C$.

Sample	BE Ni^{3+} $2p_{3/2}$ (eV)	BE Ni^{2+} $2p_{3/2}$ (eV)	Ni^{3+} FWHM (eV)	Ni^{2+} FWHM (eV)	Ni^{3+} area (%)	Ni^{2+} area (%)
x=0	856.17	854.45	2.7	2.4	57.6	42.4
x=0.3	856.12	854.55	2.7	2.4	57.2	42.8
x=0.5	856.2	854.64	2.67	2.4	48.2	51.8
x=0.7	856.1	854.5	2.61	2.4	49	51
$Mn_{0.5}Ni_{0.5}Co_2O_4/C$	856.03	854.43	2.24	2.24	45.3	54.7

Table S2

BEs (in eV), FWHM (in eV) and relative percentage areas (in %) of the four components of the C 1s core level for the $Mn_{0.5}Ni_{0.5}Co_2O_4/C$ sample.

component	BE (eV)	FWHM (eV)	area (%)
C1	284.78	1.19	52.7
C2	285.68	1.6	31
C3	287.31	1.58	7.5
C4	289.12	1.91	8.8

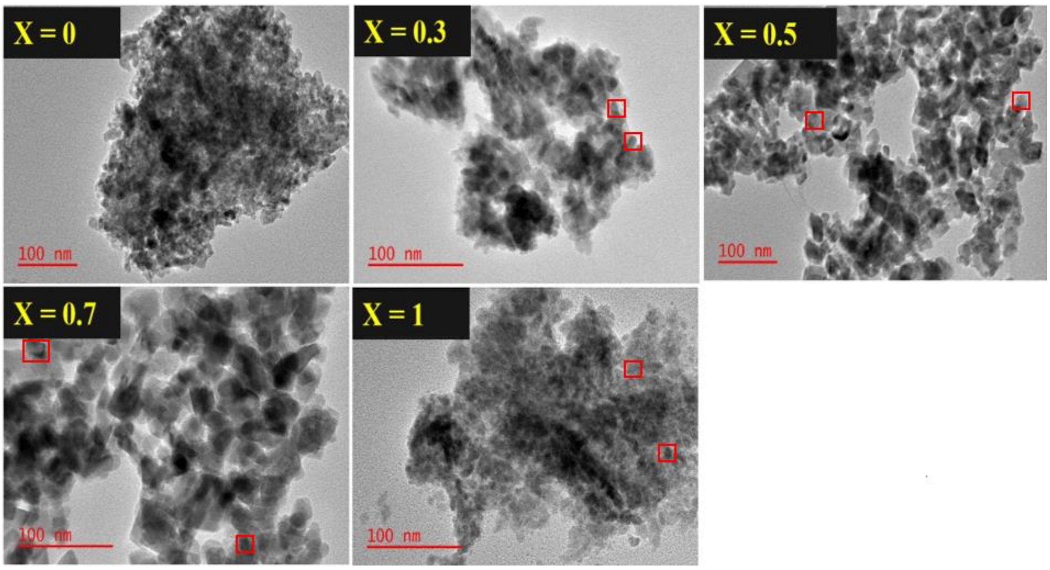

Figure S1. TEM images of $NiCo_2O_4$ (x = 0), $Mn_{0.3}Ni_{0.7}Co_2O_4$ (x = 0.3), $Mn_{0.5}Ni_{0.5}Co_2O_4$ (x = 0.5), $Mn_{0.7}Ni_{0.3}Co_2O_4$ (x = 0.7) and $MnCo_2O_4$ (x = 1).

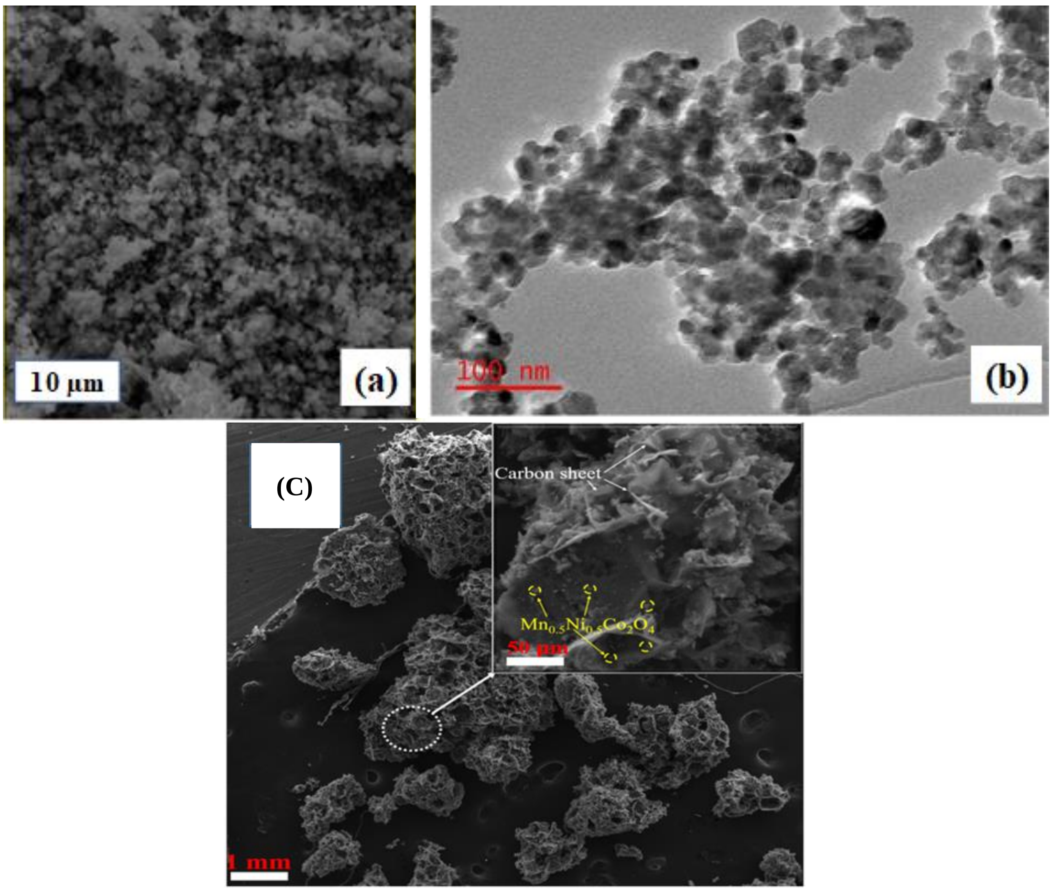

Figure S2. (a,c) $Mn_{0.5}Ni_{0.5}Co_2O_4$ and $Mn_{0.5}Ni_{0.5}Co_2O_4/C$ SEM image respectively, and **(b)** TEM image

Oxygen reduction reaction proposed mechanism:

$2M^{n+} - O^{2-} + 2H_2O + 2e^- \rightarrow 2M^{(n-1)+}{-}OH^- + 2OH^-$ Eq. S 2

$O_2 + e^- \rightarrow O_{2,\,ads}^-$ Eq. S 3

$2M^{(n-1)+}\text{-}OH^- + O_{2,\,ads}^- + e^- \rightarrow 2M^{n+}\text{–}O^{2-} + 2OH^-$ (rate determining step) Eq. S 4

Or then again with the more noteworthy likelihood

$M^{n+}\text{–}O^{2-} + H_2O + e^- \rightarrow M^{(n-1)+}\text{-}OH^- + OH^-$ Eq. S 5

$O_2 + e^- \rightarrow O_{2,\,ads}^-$ Eq. S 6

$M^{(n-1)+}\text{-}OH^- + O_{2,\,ads}^- + e^- \rightarrow M^{n+}\text{–}O^{2-} + OH^-$ Eq. S 7

$M^{n+}\text{–}O\text{–}O^{2-} + H_2O + 2e^- \rightarrow M^{(n-1)+}\text{–}O\text{–}OH^- + OH^-$ Eq. S 8

$M^{(n-1)+}\text{–}O\text{–}OH^- + e^- \rightarrow M^{n+}\text{–}O^{2-} + OH^-$ Eq. S 9

$M^{n+}\text{–}O\text{–}O^{2-} + H_2O + e^- \rightarrow M^{(n-1)+}\text{–}OH^- + HOO^-$ (rate determining step) Eq. S 10

With the above-proposed mechanism, the synthesized $Mn_xNi_{1-x}Co_2O_4$ spinel series follows [1,2]:

$Mn_xNi_{1-x}Co_2O_4 + 4OH^- + H_2O \leftrightarrow Mn_xOOH + Ni_{1-x}OOH + 2CoOOH + 4e^-$ Eq. S 11

For simplicity, note the metallic ratios have been deliberately left out in the following equations:

$CoOOH + OH^- \leftrightarrow CoO_2 + H_2O + e^-$ Eq. S 12

$2Co^{2+}OOH + O_2 \rightarrow 2(Co^{3+}OOH.O^-)$ Eq. S 13

$2(Co^{3+}OOH.O^-) + e^- \rightarrow 2Co^{3+}O_2 + 2OH^-$ Eq. S 14

$2Co^{3+}O_2 + 2H_2O + e^- \rightarrow 2Co^{2+}OOH + 2OH^-$ Eq. S 15

$Mn^{4+}O_2 + H_2O + e^- \rightarrow Mn^{3+}OOH + OH^-$ Eq. S 16

$2Mn^{3+}OOH + O_2 \rightarrow 2(Mn^{4+}OOH.O^-)$ Eq. S 17

$2(Mn^{4+}OOH.O^-) + e^- \rightarrow Mn^{4+}O_2 + OH^-$ Eq. S 18

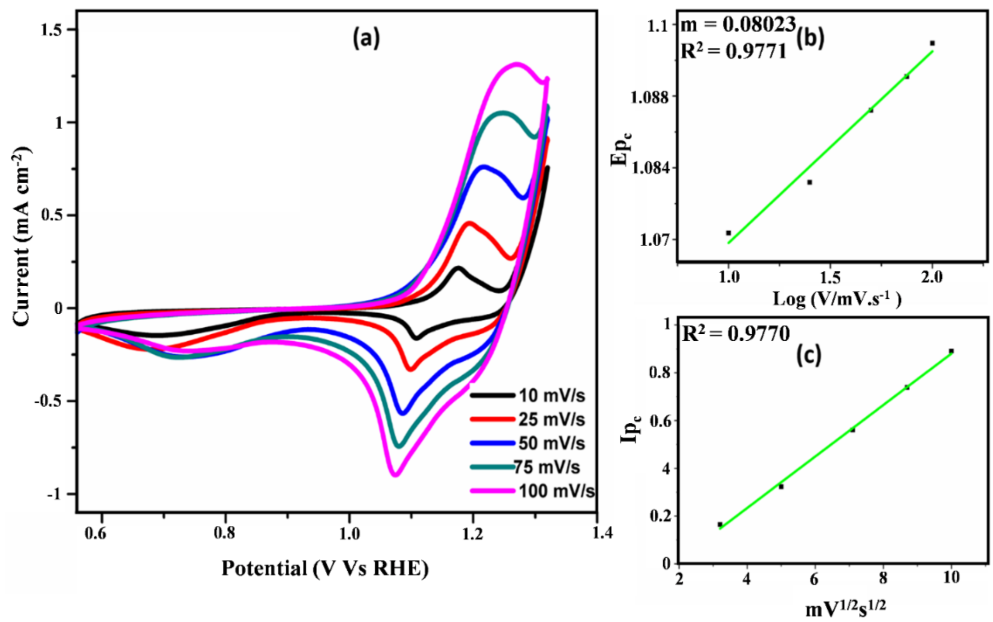

Figure S3. **(a)** Scan rate studies of $NiCo_2O_4$ electro-catalyst in O_2-saturated 0.1 M KOH at different scan rates, 10-100 mV/s **(b)** Peak current dependence on the scan rate **(c)** Peak potential dependence on the logarithmic value of scan rate.

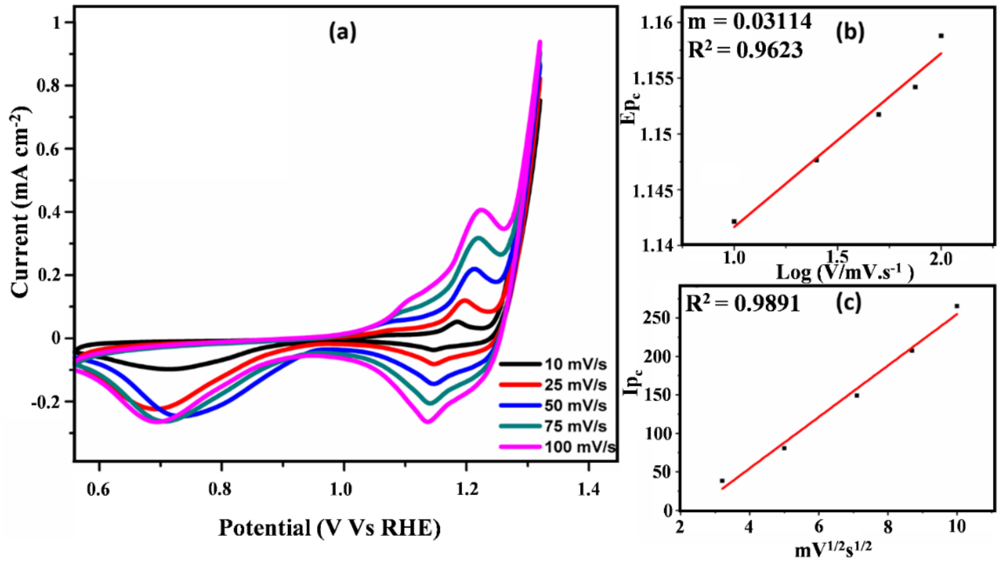

Figure S4. **(a)** Scan rate studies of $Mn_{0.3}Ni_{0.7}Co_2O_4$ electro-catalyst in O_2-saturated 0.1 M KOH at different scan rates, 10-100 mV/s **(b)** Peak current dependence on the scan rate **(c)** Peak potential dependence on the logarithmic value of scan rate.

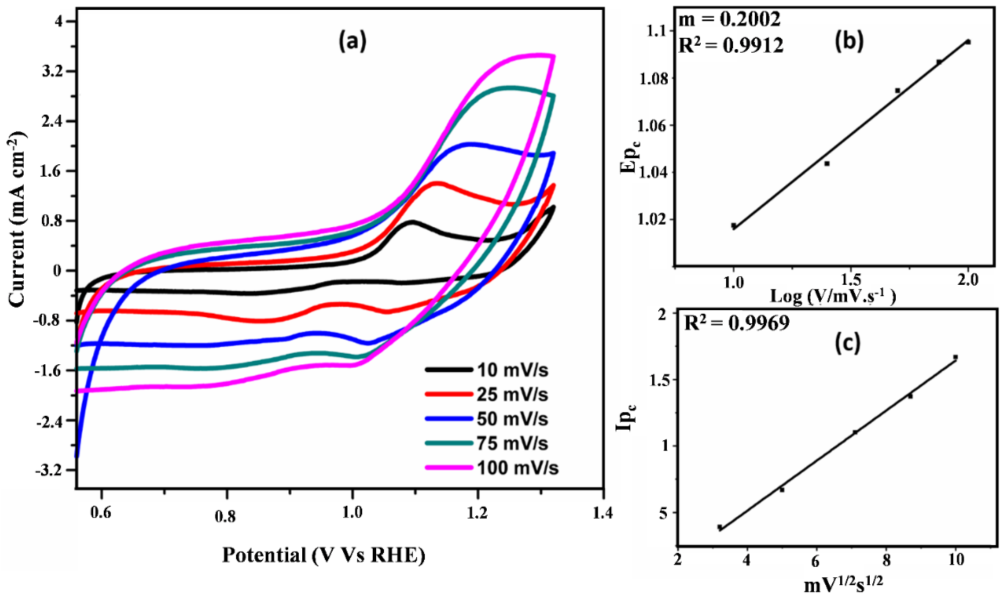

Figure S5. **(a)** Scan rate studies of $Mn_{0.5}Ni_{0.5}Co_2O_4$ electro-catalyst in O_2-saturated 0.1 M KOH at different scan rates, 10-100 mV/s **(b)** Peak current dependence on the scan rate **(c)** Peak potential dependence on the logarithmic value of scan rate.

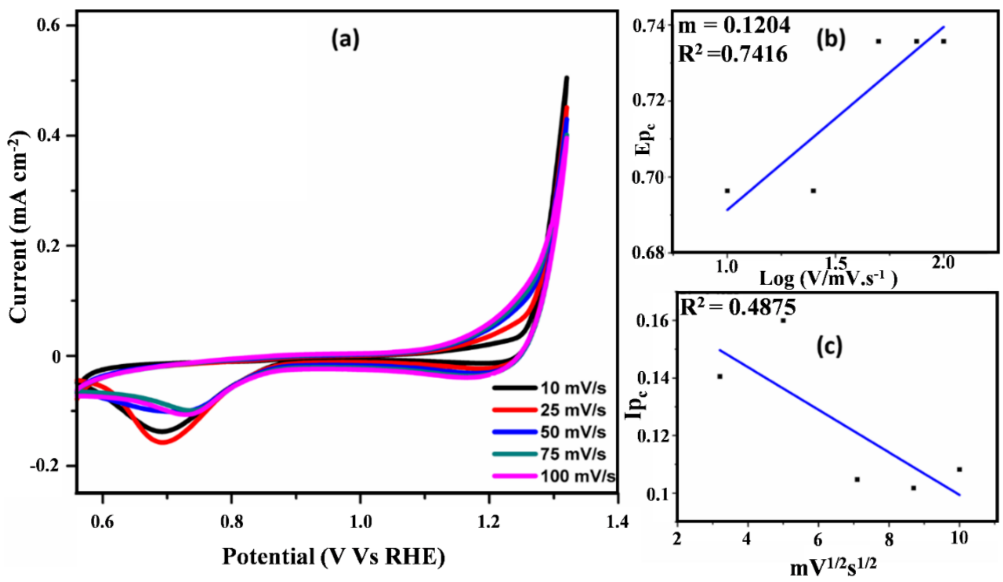

Figure S6. **(a)** Scan rate studies of $Mn_{0.7}Ni_{0.3}Co_2O_4$ electro-catalyst in O_2-saturated 0.1 M KOH at different scan rates, 10-100 mV/s **(b)** Peak current dependence on the scan rate **(c)** Peak potential dependence on the logarithmic value of scan rate.

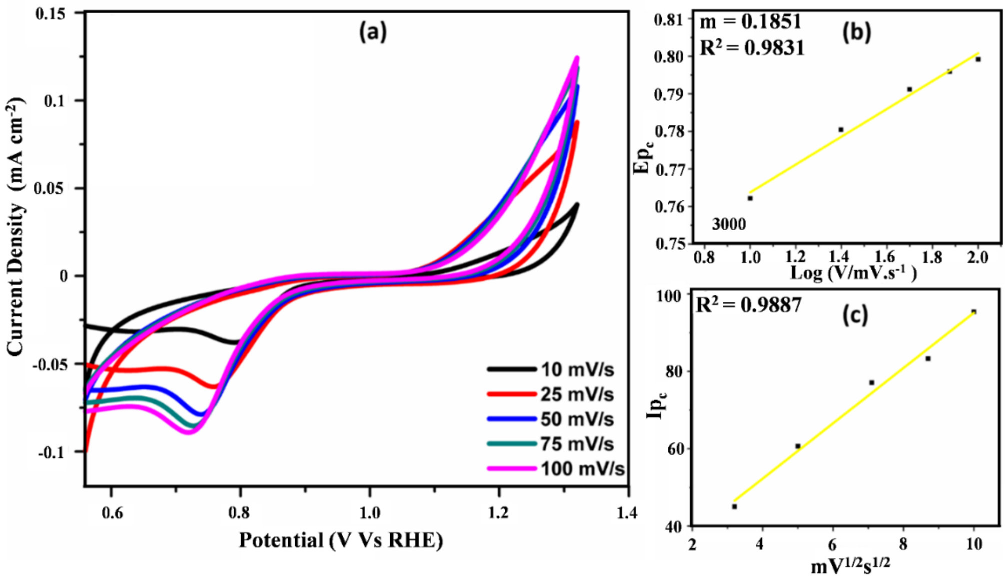

Figure S7. **(a)** Scan rate studies of $MnCo_2O_4$ electro-catalyst in O_2-saturated 0.1 M KOH at different scan rates, 10-100 mV/s **(b)** Peak current dependence on the scan rate **(c)** Peak potential dependence on the logarithmic value of scan rate.

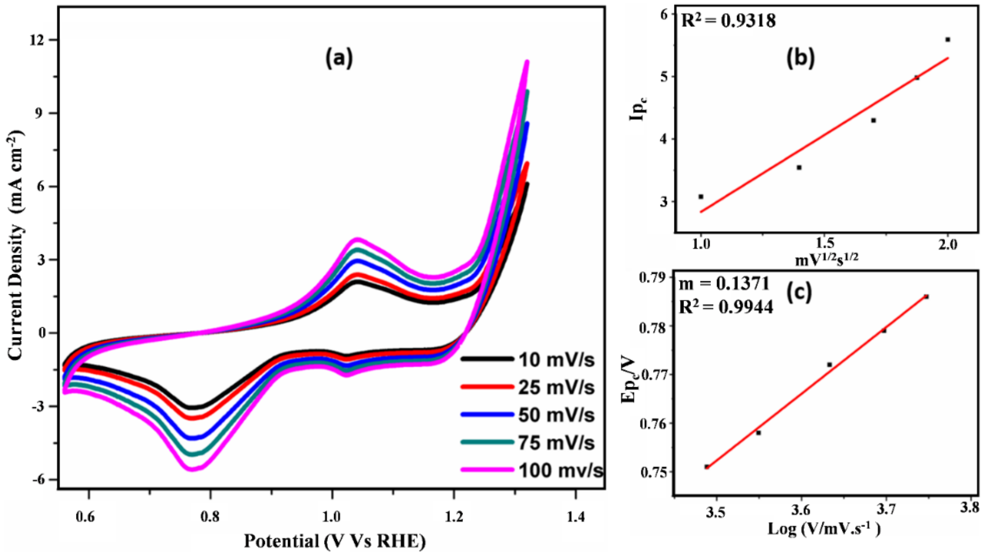

Figure S8. **(a)** Scan rate studies of $Mn_{0.5}Ni_{0.5}Co_2O_4/C$ electro-catalyst in O_2-saturated 0.1 M KOH at different scan rates, 10-100 mV/s **(b)** Peak current dependence on the scan rate **(c)** Peak potential dependence on the logarithmic value of scan rate.

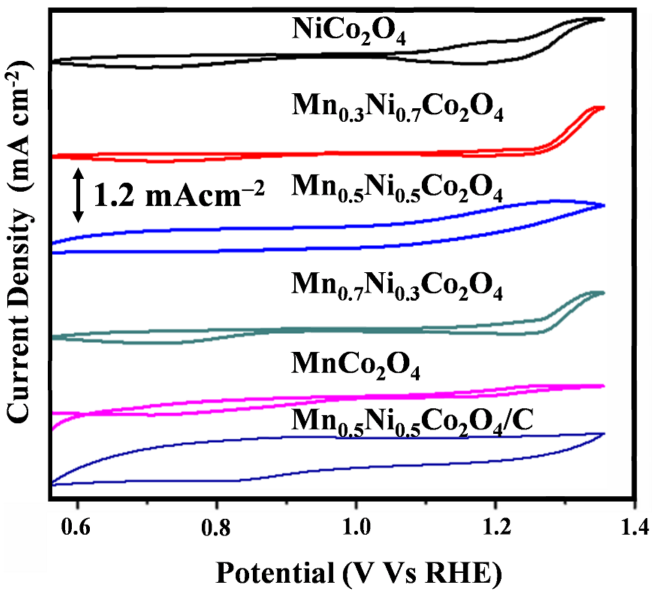

Figure S9: Cyclic Voltammetry in N_2-saturated 0.1 M KOH at 50 mVs^{-1} for $Mn_xNi_{1-x}Co_2O_4$ (x = 0, 0.3, 0.5, 0.7, and 1) and $Mn_{0.5}Ni_{0.5}Co_2O_4/C$.

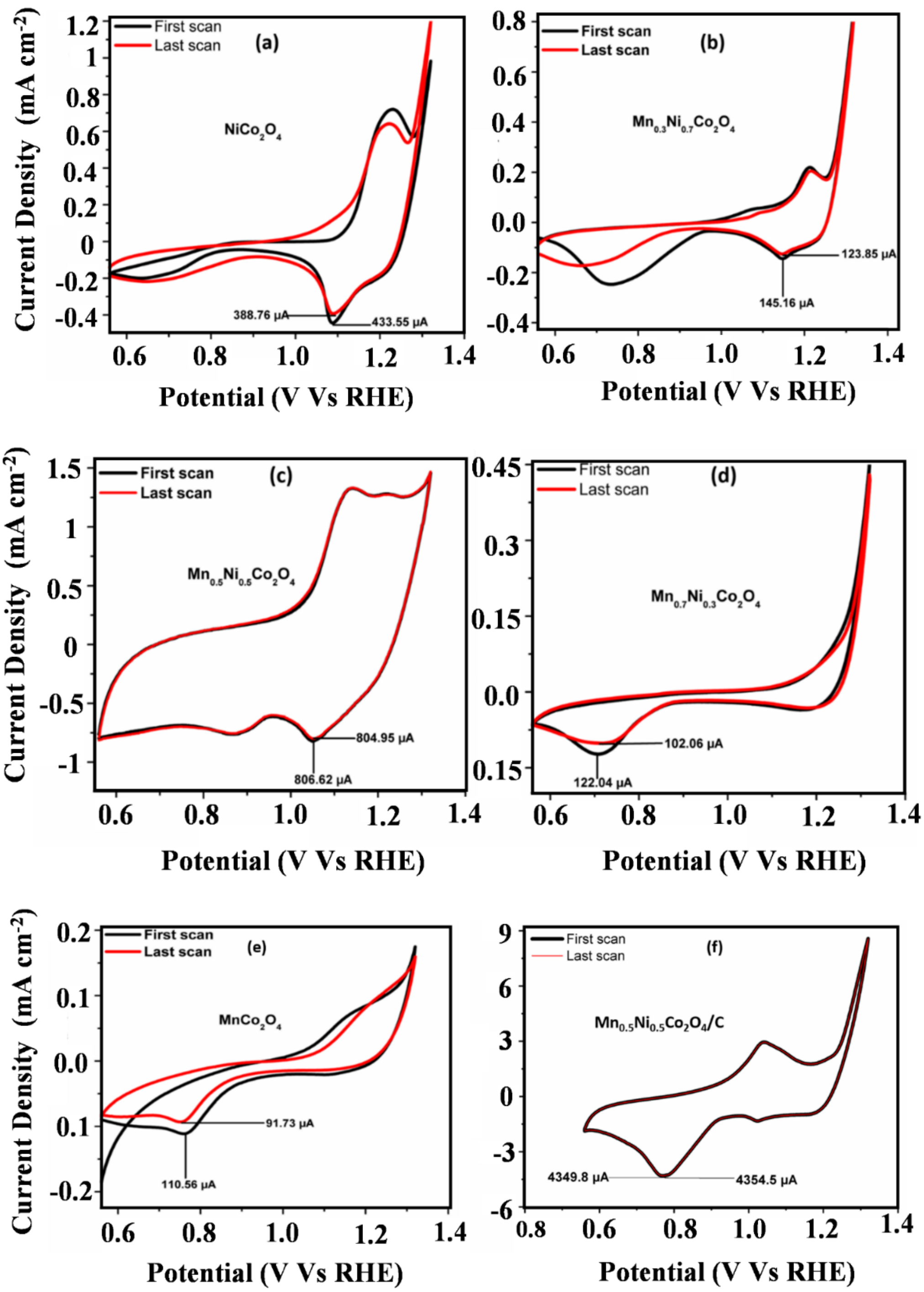

Figure S10. Durability test (405 scans) in O_2-saturated 0.1 M KOH at 50 mVs^{-1} **(a)** $NiCo_2O_4$ (b) $Mn_{0.3}Ni_{0.7}Co_2O_4$ **(c)** $Mn_{0.5}Ni_{0.5}Co_2O_4$ **(d)** $Mn_{0.7}Ni_{0.3}Co_2O_4$ **(e)** $MnCo_2O_4$ **(f)** $Mn_{0.5}Ni_{0.5}Co_2O_4$/C.

Table S3.

Electrocatalytic performance of the synthesized electro-catalysts for the oxygen reduction reaction and percentage current loss as calculated from cyclic voltammogram data.

Electro-catalysts	**$NiCo_2O_4$**	**$Mn_{0.3}Ni_{0.7}Co_2O_4$**	**$Mn_{0.5}Ni_{0.5}Co_2O_4$**	**$Mn_{0.7}Ni_{0.3}Co_2O_4$**	**$MnCo_2O_4$**	**$Mn_{0.5}Ni_{0.5}Co_2O_4$/C**
Tafel slope,b (mV/dec)	0.161	0.0623	0.400	0.241	0.370	0.274
***Current loss (%)**	12.30	14.68	0.21	16.37	17.03	0.11

$m = \frac{b}{2}$, b Tafel slope

Tafel slopes values for the cathodes were calculated from the linear fitting results of scan rate

*Current loss $(\%) = \frac{\text{First scan peak current } (\mu A)}{\text{last scan peak current } (\mu A)} \times 100\%$

Table S3.

Comparison of oxygen reduction reaction electroactivities of electrocatalyst in this work with reported electrocatalysts.

Spinel	Synthesis method	Feature/strategies	Reaction medium	$^{a}E_{\frac{1}{2}}$ (V)	^{b,c}Current density (mA/cm^2)	Stability (Chrono-am-perometric current loss)	Ref
$Cu_xCo_{3-x}O_4$	one-step hydro-thermal	Encapsulation in carbon nanomaterials more oxygen vacancies	Alkaline (0.1 M KOH)	0.82	~6.3	12.32% af-ter 12000s	[1]
$CoIn_2Se_4$	polyol solution reduction	abundant active sites and ideal charge trans-fer	Alkaline (0.1 M KOH)	0.77	~5.0	--	[2]
$CoCuMnO_x$	modified sacrifi-cial template	single-phase multiple functionality	Alkaline (0.1 M KOH)	~0.83	~6.2	~10% after 10000s	[3]
$CoFe_2O_4$ /car-bon nano-tube	solvothermal and calcination	coupling effect	Alkaline (0.1 M KOH)	0.808	~5.4	5.41% after 20000s	[4]
$CoIn_2S_4$/S-rGO	in situ solvother-mal growth pro-cess	open and porous hierar-chical structure	Alkaline (0.1 M KOH)	0.83	~ 5.8	17.8% after 5000s	[5]

Fe-Co/N,S-MPC	microwave-assisted hydrothermal route	Support material heteroatom doping	Alkaline (0.1 M KOH)	0.78	~4.25	-	[6]
AlCoMn	Metal-melt-spinning	Dealloying	Alkaline (0.1 M KOH)	~0.80	~6.1	-	[7]
$Co_{0.5}Fe_{0.5}S_4$	facile soft template	coupling interaction and encapsulation	Alkaline (0.1 M KOH)	~0.808	~6.4	11%	[8]
$CoV_{2-x}FexO_4$	Thermal decomposition	Cationic substitution	Alkaline (1 M KOH)	~0.9	~3.65	-	[9]
$Mn_{0.5}Ni_{0.5}Co_2O_4$/C	**template assisted citrate sol-gel**	**synergism and metallic cooperation**	**Alkaline (1 M KOH)**	**0.856**	**5.54**	**11.4%**	**This work**

1. Kumar, R.; Singh, L.; Wahid, Z.A.; Mahapatra, D.M.; Liu, H. Novel mesoporous MnCo2O4 nanorods as oxygen reduction catalyst at neutral pH in microbial fuel cells. *Bioresour. Technol.* **2018**, *254*, 1–6, doi:10.1016/j.biortech.2018.01.053.

2. Ko, T.H.; Radhakrishnan, S.; Seo, M.K.; Khil, M.S.; Kim, H.Y.; Kim, B.S. A green and scalable dry synthesis of NiCo2O4/graphene nanohybrids for high-performance supercapacitor and enzymeless glucose biosensor applications. *J. Alloys Compd.* **2017**, *696*, 193–200, doi:10.1016/j.jallcom.2016.11.234.

3. Jin, W.; Chen, J.; Wu, Z.; Maduraiveeran, G. Encapsulated spinel CuXCo3-XO4 in carbon nanotubes as efficient and stable oxygen electrocatalysts. *Int. J. Hydrogen Energy* **2019**, *44*, 11421–11430, doi:10.1016/j.ijhydene.2019.03.093.

4. Wang, J.; Zheng, X.; Cao, Y.; Li, L.; Zhong, C.; Deng, Y.; Han, X.; Hu, W. Developing Indium-based Ternary Spinel Selenides for Efficient Solid Flexible Zn-Air Batteries and Water Splitting. *ACS Appl. Mater. Interfaces* **2020**, *12*, 8115–8123, doi:10.1021/acsami.9b18304.

5. Huang, K.; Liu, J.; Wang, L.; Chang, G.; Wang, R.; Lei, M.; Wang, Y.; He, Y. Mixed valence CoCuMnOx spinel nanoparticles by sacrificial template method with enhanced ORR performance. *Appl. Surf. Sci.* **2019**, *487*, 1145–1151, doi:10.1016/j.apsusc.2019.05.183.

6. Huang, Q.; Li, C.; Tu, Y.; Jiang, Y.; Mei, P.; Yan, X. Spinel CoFe2O4 /carbon nanotube composites as efficient bifunctional electrocatalysts for oxygen reduction and oxygen evolution reaction. *Ceram. Int.* **2021**, *47*, 1602–1608, doi:10.1016/j.ceramint.2020.08.276.

7. Fu, G.; Wang, J.; Chen, Y.; Liu, Y.; Tang, Y.; Goodenough, J.B.; Lee, J.M. Exploring Indium-Based Ternary Thiospinel as Conceivable High-Potential Air-Cathode for Rechargeable Zn–Air Batteries. *Adv. Energy Mater.* **2018**, *8*, 1–12, doi:10.1002/aenm.201802263.

8. Kostuch, A.; Gryboś, J.; Wierzbicki, S.; Sojka, Z.; Kruczała, K. Selectivity of mixed iron-cobalt spinels deposited

on a n,s-doped mesoporous carbon support in the oxygen reduction reaction in alkaline media. *Materials (Basel).* **2021**, *14*, 1–19, doi:10.3390/ma14040820.

9. Li, S.; Zhou, X.; Fang, G.; Xie, G.; Liu, X.; Lin, X.; Qiu, H.J. Multicomponent Spinel Metal Oxide Nanocomposites as High-Performance Bifunctional Catalysts in Zn-Air Batteries. *ACS Appl. Energy Mater.* **2020**, *3*, 7710–7718, doi:10.1021/acsaem.0c01121.

10. Shen, M.; Ruan, C.; Chen, Y.; Jiang, C.; Ai, K.; Lu, L. Covalent entrapment of cobalt-iron sulfides in N-doped mesoporous carbon: Extraordinary bifunctional electrocatalysts for oxygen reduction and evolution reactions. *ACS Appl. Mater. Interfaces* **2015**, *7*, 1207–1218, doi:10.1021/am507033x.

11. Chakrapani, K.; Bendt, G.; Hajiyani, H.; Lunkenbein, T.; Greiner, M.T.; Masliuk, L.; Salamon, S.; Landers, J.; Schlögl, R.; Wende, H.; et al. The Role of Composition of Uniform and Highly Dispersed Cobalt Vanadium Iron Spinel Nanocrystals for Oxygen Electrocatalysis. *ACS Catal.* **2018**, *8*, 1259–1267, doi:10.1021/acscatal.7b03529.